Properties of PMMA end cap holders affect FE stiffness predictions of vertebral specimens

Journal Title
XX(X):1–8

DOI: 10.1177/ToBeAssigned
www.sagepub.com/
SAGE

Bruno Agostinho Hernandez[1], PhD, Harinderjit S. Gill[1], DPhil, and Sabina Gheduzzi[1], PhD.

Abstract

Bone cement is often used, in experimental biomechanics, as a potting agent for vertebral bodies (VB). As a consequence, it is usually included in finite element (FE) models to improve accuracy in boundary condition settings. However, bone cement material properties are typically assigned to these models based on literature data obtained from specimens created under conditions which often differ from those employed for cement end caps. These discrepancies can result in solids with different material properties from those reported. Therefore, this study aimed to analyse the effect of assigning different mechanical properties to bone cement in FE vertebral models. A porcine C2 vertebral body was potted in bone cement end caps, μCT scanned, and tested in compression. DIC was performed on the anterior surface of the specimen to monitor the displacement. Specimen stiffness was calculated from the load-displacement output of the materials testing machine and from the machine load output and average displacement measured by DIC. Fifteen bone cement cylinders with dimensions similar to the cement end caps were produced and subjected to the same compression protocol as the vertebral specimen and average stiffness and Young' moduli were estimated. Two geometrically identical vertebral body FE models were created from the μCT images, the only difference residing in the values assigned to bone cement material properties: in one model these were obtained from the literature and in the other from the cylindrical cement samples previously tested. The average Young's modulus of the bone cement cylindrical specimens was 1177$\pm$3 MPa, considerably lower than the values reported in the literature. With this value, the FE model predicted a vertebral specimen stiffness 3% lower than that measured experimentally, while when using the value most commonly reported in similar studies, specimen stiffness was overestimated by 150%.

Keywords

PMMA Bone Cement, Finite Element Model, Vertebral bodies.

Introduction

Polymethyl methacrylate (PMMA) bone cement is extensively used in orthopaedic surgery for fixation of prostheses and to enhance screw stability[4,23]. It is also widely used in experimental biomechanical tests as a potting agent, as it is readily available and is easily moulded into specimen specific fixtures[18,27,30]. As a consequence, bone cement end caps are often included in specimen specific Finite Element (FE) models, particularly in spine studies, to increase geometrical and boundary condition accuracy[17–19,21,27,31].

The Young's modulus of bone cement is reported to range from 2.1 to 3.1 MPa, depending on cement type, brand and on the procedure followed during mixing[8,10,23,25]. The determination of bone cement compressive mechanical properties is usually made using short and thin cylindrical samples following ISO 5833:2002[2], therefore ensuring relatively uniform cooling as well as homogeneous and continuous properties[23].

Particularly for spine studies, while the majority of cement specimen holders prepared for experimental work are still cylindrical, they are considerably larger[3,6,12,14,17,44,45]. Such change in dimensions could potentially generate differences in the final mechanical properties, such as material stiffness, as there would be a cooling gradient across the cement and air could be readily trapped inside the mould, giving rise to significant porosity and consequent depletion of mechanical properties[4,11,23,39].

A variation in the mechanical properties of the cement end caps could have a considerable effect on the numerical results of FE models, as the influence of load application and boundary conditions on FE vertebral body models has been found to be significant[18]. In particular, the correct application of boundary conditions increases the accuracy of the FE models. Therefore, ensuring that the contact between specimen and fixtures is correctly represented and that the mechanical properties of the fixtures material are correctly defined would improve the accuracy of the numerical models, and would allow focus on more important experiment specific parameters, such as the accurate definition of bone material properties.

Recently, Digital Image Correlation (DIC) has seen increased levels of popularity in experimental biomechanics, mainly due to its non-invasive nature and its ability to output field measurement of both strain and displacement. These

[1]Centre for Orthopaedics Biomechanics, Department of Mechanical Engineering, University of Bath, Bath, United Kingdom.

Corresponding author:
Harinderjit S. Gill, Centre for Orthopaedics Biomechanics, Department of Mechanical Engineering, University of Bath, Bath, United Kingdom.
Email: R.Gill@bath.ac.uk

two characteristics afford DIC considerable advantages over more traditional techniques, and this is especially important when dealing with samples characterised by complex geometries such as vertebral bodies [13,32,33,38].

This study aimed to analyse the effect of the compressive mechanical properties of bone cement specimen holders on the stiffness prediction of finite element models of vertebral bodies.

Materials and Methods

Experimental Procedure

A C2 cervical vertebra was dissected from a juvenile porcine spine obtained from a local butcher and cleaned of all soft tissues. Transverse and posterior processes were removed so to isolate the vertebral body (VB). PMMA bone cement (Simplex Simplex, Stryker Ltd, Newbury, United Kingdom) was mixed by hand at a room temperature of 15° using a bowl and spatula mixing kit (HIGHVAc BOWL, Summit Medical, Bourton on the Water, UK). Care was taken to ensure the mixing frequency fell within 1 to 2 Hz to minimize air entrapment; mixing time varied between 45 to 120 seconds [23]. The mixed cement was poured into a cylindrical PTFE mould of 50 mm diameter and 15 mm depth and the porcine VB was lowered onto it ensuring good coverage of the endplate had been achieved, while, at the same time, maintaining it parallel with the horizontal. The cement was left to cure for 30 minutes while the VB was held in position using a laboratory specimen stand. After curing, the sample was turned upside down and the second endplate was lowered onto another PTFE cement filled mould following the same procedure. Once both cement end caps had cured the PTFE moulds were removed and the sample was μCT scanned, alongside two phantoms, at a voxel size of 0.1 mm using a Nikon XTH225ST Micro-CT Scanner Unit (Nikon Metrology Inc, Michigan, USA). The anterior aspect of the sample was covered with a layer of white paint and a black speckle pattern was applied to allow DIC measurements to be performed.

In addition to the VB sample, fifteen bone cement cylinders (n=15) were produced using the same cement brand, procedure and equipment used to create the vertebral end caps; after mixing the cement was poured into the PTFE moulds and left to solidify. After 30 minutes, the now solid cement was removed from the moulds, machined to ensure that both top and bottom sides were flat and parallel, and sequentially numbered. The PMMA cylinders were μCT scanned using the same parameters used for the vertebral sample while their characteristic dimensions, i.e. length and diameter, were measured five times using a digital calliper having a resolution of 0.01 mm.

The vertebral sample and the fifteen cement cylinders were tested in axial compression using a 30 kN. materials testing machine (Instron 5967, High Wycombe, United Kingdom). Each specimen was positioned in the centre of the machine baseplate and, in order to avoid any local deformations and to ensure that a uniform load would be applied, a steel plate was placed between the cement (this either being the top face of one of the cylinders or the flat face of the vertebral specimen cement end caps) and the crosshead of the materials testing machine (Figures 1 and 2a). A compressive ramp was applied at a rate of 1000 Nmm^{-1} , up to a maximum load of 10 kN, via a push rod. The push rod had a rounded end to reduce the contact area on the steel plate and to minimise the effect of possible misalignments. Load displacement curves were plotted for all samples. Stiffness was evaluated between the loads of 3 to 5 kN, i.e. the most linear part of the curves, using a custom algorithm developed within Matlab (v2016b, MathWorks Inc., Massachusetts, United States).

In the case of the cylindrical PMMA specimens, their known geometry allowed to plot stress-strain curves from which Young's modulus was calculated. Average values for cement stiffness and Young's modulus for the group were calculated, weighted by the reciprocal of the standard error of the slope of the line of best fit [42].

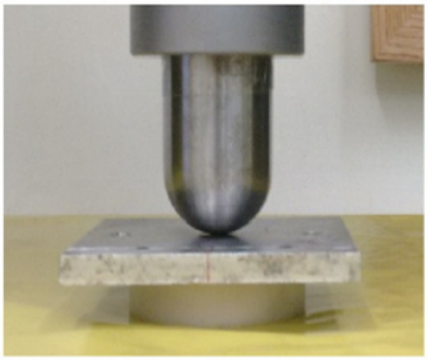

Figure 1. Bone cement sample loading set-up including steel plate and push rod attached to the crosshead of the materials testing machine.

The loading response of the vertebral sample was further analysed using DIC. Briefly, a single GigE DFK 23GP01 digital camera (The Imaging Source Europe GmbH, Germany) was positioned perpendicularly to the anterior surface of the VB. During compression one image was acquired every 5 seconds using a custom MatLab code (MathWorks, Massachusetts, USA). Ncorr V2.1 [1], a Matlab based open source function, was used to calculate the displacement field on two regions of interest (RoIs) defined on the surface of the superior cement end-cap, close to the point of application of the load, and on the anterior part of the vertebral body, respectively (Figure 2a). The average vertical displacement on each RoI was plotted alongside the testing machine load-cell data, thus allowing investigation of the loading response of different portions of the sample; namely displacement data obtained from the superior cement cap RoI allowed to infer the combined stiffness of the whole sample, i.e. the combined stiffness arising from the superior cement cap, vertebral body and inferior cement cap (denoted K1, in Figure 2a); the vertebral body RoI allowed to estimate the combined stiffness arising from the vertebral body itself and the inferior cement cap (denoted K2 in Figure 2a).

Numerical Model

The influence of the material properties of the cement end caps on predicted stiffness was studied by means of a specimen-specific FE model of the vertebral sample tested experimentally, Figure 2b. The geometrical model was created from the previously acquired μCT image via ScanIP (v2017-18 Simpleware Synopsys, California, USA)

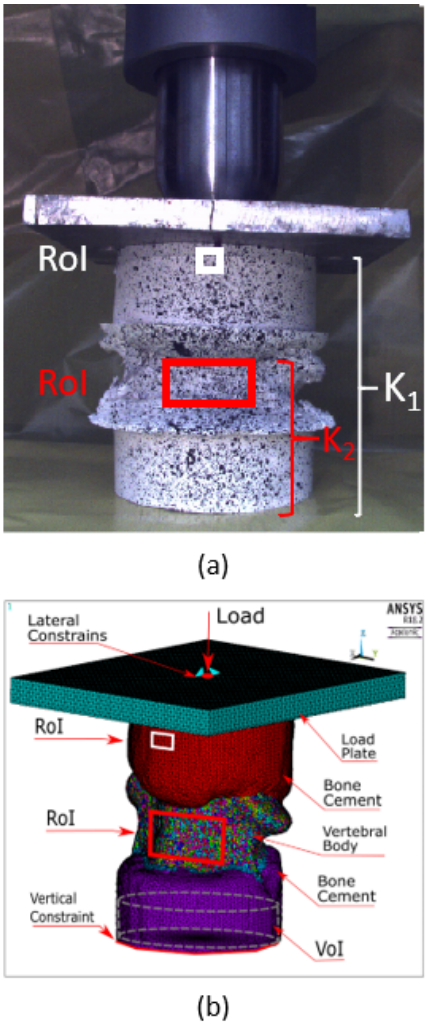

Figure 2. Regions of Interest (RoI) and Volume of Interest (VoI). (a) Vertebral body sample prepared for DIC with the two different RoIs clearly marked. Each RoI allows the loading response of different parts of the specimen to be isolated. The top RoI (white outline) is defined on the superior cement cap, its displacement combined with the applied load will allow an estimate of the stiffness of the whole sample comprising the two cement end caps and VB (K_1); the second, middle RoI (red outline) is defined on the anterior surface of the VB and will allow an estimate of the combined stiffness arising from the VB and the inferior cement end cap (K_2). (b) Vertebral sample specimen-specific finite element model, applied boundary conditions and delineation of RoIs and VoIs used for stiffness comparisons with experimental DIC data.

and included the upper and lower bone cement holders, the C2 vertebral body, any cartilage remaining from dissection and the steel plate used to apply the load thus replicating the experimental set-up.

Model generation involved software tools such as flood filling, thresholding, painting, filtering and interpolation to create smooth geometries from the μCT image, while boolean operators were used to obtain a perfect contact interface between parts. Sections of the cartilage were only included in the model when tissue thickness exceeded three pixels, as recommended by software guidelines[41].

The element types chosen for this study were a mixture of hexahedrons, to represent the internal trabecular structure orientation, and tetrahedrons, to represent and smoothen the external surface[6,16,31,36]. The geometrical model was converted into FE numerical model and solved using ANSYS Mechanical ADPL (v18.2, ANSYS Inc, USA) installed on a Xeon 32 cores, 120Gb ram PC.

Bone cement, trabecular bone and steel were modelled as isotropic and linear materials while cartilage was assigned as a hyper-elastic material[37] (Table 1). The properties for cartilage and steel were based on literature data; while cancellous bone properties were obtained from the grey-scale of the μCT image, adjusted with the phantoms' grey-scale, using a standard relationship[15,20]. Based on this VB model, two simulations were conducted: one using the Young's modulus value for bone cement obtained from the experiments performed in the current study and another one using data from the literature.

Table 1. Material properties used in the numerical model.

Body	Type	Elastic Component (MPa)	Poisson's ratio	Reference
Cartilage	Hyperelastic Neo-Hookean	C_{10} = 0.3448 D_1 = 0.3	-	37
Cement	Isotropic	3000	0.3	6
Steel Plate	Isotropic	200,000	0.3	22

The same load parameters as per the experiment were used in the FE study: a compressive load was applied at a rate of 1000 N/min on the plate up to a maximum of 10 kN. The point of application of the load corresponded to that used during the experiments and it was identified by measuring the distance of the point of contact of the push rod from the edge of the cranial specimen holder. For each VB FE model, three load-displacement curves were generated. The first two were obtained by plotting the reaction loads against the average vertical displacement of element nodes corresponding to the two RoIs used experimentally (Figure 2b). Stiffness values K_1 and K_2 were calculated from the linear portion of such load-displacement curves and compared to DIC experimental findings. The third set of curves were generated by plotting the average displacement of a volume of interest (VoI) having the same geometry and dimensions as the experimental cement cylinders, placed within the bottom cement end cap and loaded via the vertebral body. Stiffness calculated from this volume of interest (denoted K_{cement}) was compared to the average experimental stiffness value obtained from the 15 cement cylinders.

Results

Experimental Results

The cement samples stiffness ranged from 112,690 to 176,270 Nmm^{-1} , with a weighted average for this group of 141,160$\pm$33 Nmm^{-1} . The stress-strain curves for the 15 bone cement samples (Figure 3) were obtained from the load-displacement output of the material testing machine and each sample characteristic geometry. Young's modulus was calculated in the range 3.5 to 5 MPa from the slope of line of best fit through the experimental data point and ranged from 778 to 1,586 MPa. The weighted value of Young's modulus for the whole dataset was 1,177$\pm$3 MPa.

Three load displacement curves were produced for the vertebral body specimen in the experiment. The first and

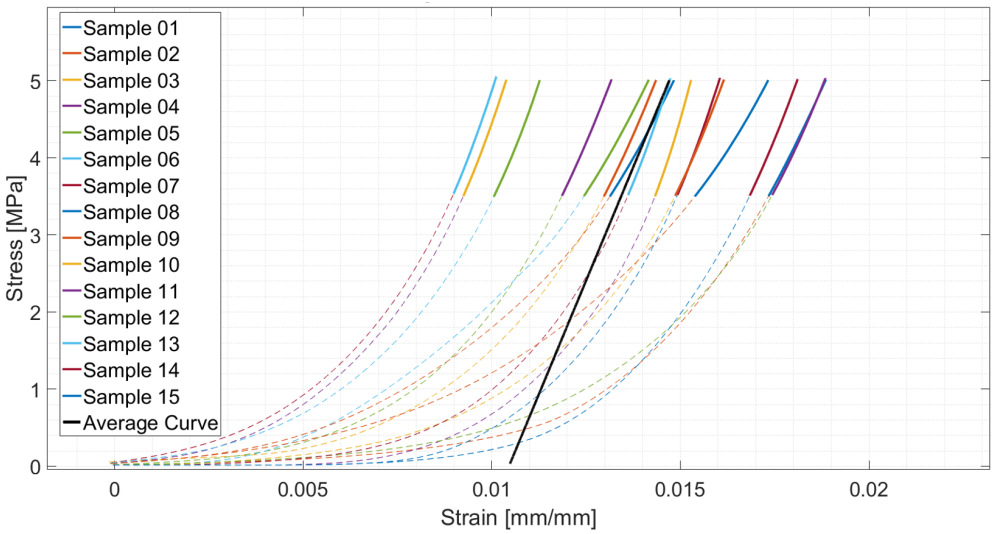

Figure 3. Stress-Strain curves for all samples. The bold sections are the linear sections of the curves and the black line is the weighted averaged curve.

second curve were obtained by plotting the machine load-cell output against the average displacement evaluated by DIC on the top end cap (K_1) and vertebral body (K_2) RoIs, respectively. The corresponding stiffness values are summarised in Table 2. The final load displacement curve was obtained from the load and displacement output of the materials testing machine; this allowed an alternative estimate of K_1.

Table 2. Predicted and measured stiffness values. (*) Denotes experimentally measured stiffness of cement cylinder of dimensions equivalent to the bottom end cap in the FEA models.

	DIC	FEA (Ecement = 1,177 MPa)	FEA (Ecement = 3000 MPa)	Instron
K_1 ($\mathbf{Nmm^{-1}}$)	1,949	2,844	4,448	2,947±6
K_2 ($\mathbf{Nmm^{-1}}$)	6,484	6,415	8,060	–
K_{Cement} ($\mathbf{Nmm^{-1}}$)	–	105,110	269,310	141,160±33(*)

The load-displacement curve obtained using data from DIC on the RoI defined on the VB resulted in unrealistic specimen behaviour at a load greater than 6 kN (Figure 4). This was due to blood seeping out of the specimen, disrupting the speckle pattern and resulting in the DIC algorithm to output non-physical displacements. Data prior to this load magnitude was unaffected by this issue as confirmed by visual examination of each image.

Analysis of the μCT images of the cylindrical cement samples revealed a significant level of porosity in the centre of the sample and near to the top surface which was exposed to open air during curing. Similar porosity, both in terms of pore size and distribution, was noted in both end caps of the vertebral sample (Figure 5).

Numerical Results

A mesh sensitivity study was performed to check for convergence of the solution, resulting in a 1 mm element size. This resulted in two models comprising 486081 elements each, one where cement properties were assigned based on the average value of Young's modulus obtained experimentally in this study and one with the value obtained from the literature.

Stiffness values were calculated from both models using the reaction forces and the vertical movement of three regions of interest, and resulted in estimates for K_1, K_2 and K_{Cement} of 2,844 $\mathrm{Nmm^{-1}}$, 6,415 $\mathrm{Nmm^{-1}}$ and 105,110 $\mathrm{Nmm^{-1}}$, respectively, when cement properties were assigned in the FE model based on our experimental value; and 4,448 $\mathrm{Nmm^{-1}}$, 8,060 $\mathrm{Nmm^{-1}}$ and 269,310 $\mathrm{Nmm^{-1}}$ when cement properties were assigned based on literature data, respectively (Figure 4 and Table 2).

Discussion

This study investigated the effect of the material properties assigned to cement end caps on FE models aimed at predicting the response of a vertebral body construct to quasi-static loading. FE is widely used in biomechanical investigations and recent studies have focused on the determination of the right approach to describe the material properties of the biological elements of said models, such as cancellous bone, cartilage, etc[5,7,9,29,35,40,43]; much less attention has been paid to other elements comprising the models, such as cement end caps.

Cement end caps are widely used in experimental spine biomechanics studies[18,27,30]; this practice arises from the desire of aligning the vertical axis of vertebral bodies, typically characterised by awkward geometries, to the line of action of the applied force and avoiding point loading. In order to correctly represent the boundary and contact conditions seen experimentally it is common practice to also include cement end caps within FE models[17–19,21,27,31].

Compared to the approach adopted to model biological materials, much less importance has been given to correctly set the material properties of the bone cement, with properties typically being taken directly from the literature[8,10,25,26]. While adequate when applied to generic models, this approach fails to perform satisfactorily when good agreement with experimental data is sought in specimen-specific FE models. We hypothesised that the generic material properties assigned to bone cement in

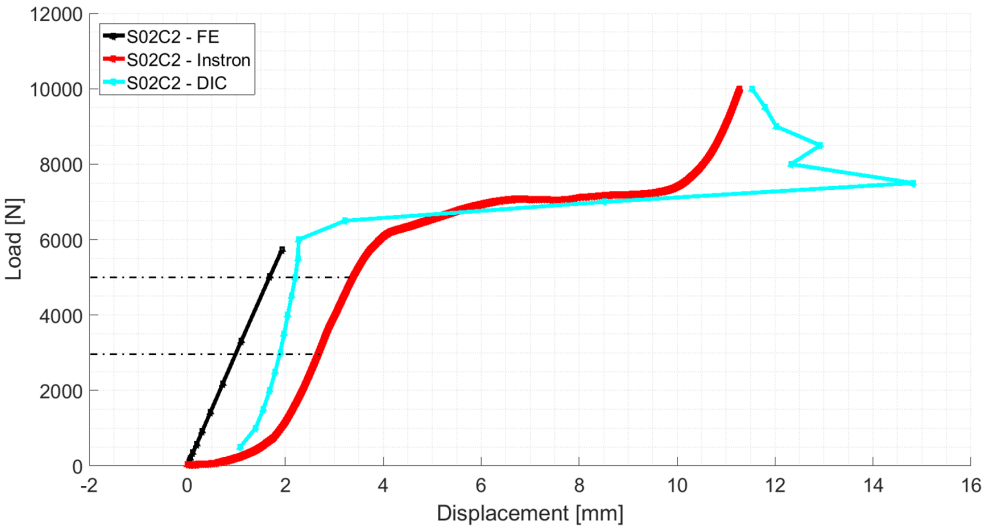

Figure 4. Load-Displacement curves for K_1 from the FE model with Young's modulus for the bone cement end cap holders of 1,177 MPa. Stiffness values were obtained in the most linear section, i.e. between 3 to 5 kN.

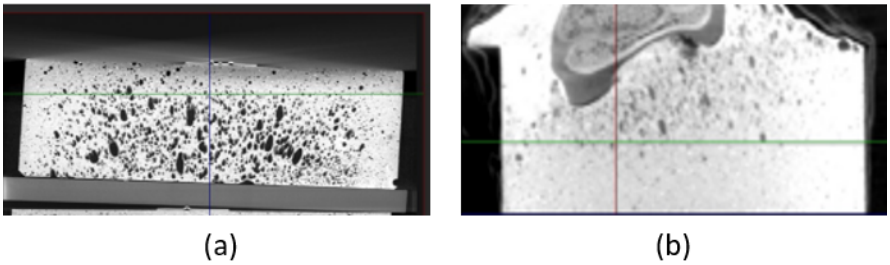

Figure 5. Cross-sectional view of one of the cement samples (a) and cross sectional view of the caudal cement end cap (b).

specimen specific models contribute to the discrepancies between numerical predictions and experimental data.

In this study fifteen bone cement samples, with dimensions comparable to cement end caps, were prepared in the open air and following a standardised mixing protocol[23]; the same procedure was used to create cement end caps onto which the porcine cervical VB was mounted. Each of the 15 cement samples was subject to a quasi-static loading ramp and the average Young's modulus for the group was calculated to be 1177 MPa, under half the value commonly reported in the literature and typically used in FEA investigations[4,22,23,34,39].

An unusual level and distribution of porosity within the cement was evidenced in the present study (Figure 5). Here cement was mixed by hand, however this practice has been shown not to increase porosity in the solidified material when compared to vacuum-mixing[24,28]. We therefore attribute this unusual presentation to the physical size of the samples and the way in which they were produced.

Mechanical tests to determine the properties of bone cement are usually conducted on small cylinder of 5 mm diameter and 12 mm height (ISO 5833:2002)[2], typically produced by pressing doughy cement into open ended cavities created within metal moulds. The metallic material, typically stainless steel, prescribed for mould construction and mould geometry (i.e. with two open ends) decrease the risk of air entrapment during specimen creation. Furthermore, the high thermal conductivity of the mould might contribute to a decrease of the temperature gradient within the sample, reducing the porosity gradient within the cement. On the other hand, bone cement end caps are usually large, with a diameter often in excess of 50 mm[3,6,12,14,17,44,45] and are typically produced within polymer moulds, hence characterised by low thermal conductivity (at least compared to metals), which are sealed at one end to prevent cement leakage. The combination of mould size, its closed geometry and material all result in unfavourable conditions for the cement, with a high likelihood of a temperature gradient arising during polymerisation and air possibly being trapped within the polymer.

Having established an experimental value of Young's modulus for cement specimens created following the same procedure as the specimen holder end-caps, the next step of the investigation focused on comparing the experimental and predicted response of the vertebral specimen to quasi-static loading. Two specimen specific models were created from the μCT image of the tested specimen. In the models material properties were assigned to cancellous bone based on image grey-scale values using a validated relationship[15,20], steel and cartilage material properties were obtained from the literature, while bone cement properties were assigned either based on the experimental results of the first part of this investigation or on literature data. Stiffness predictions were obtained from the two models for the two RoIs outlined in Figure 2 (K_1 and K_2) and for a volume of interest (VoI) contained within the bottom end cap and having dimensions comparable to the cement cylinders used in the first part of this study (K_{cement}).

DIC was used to isolate the experimentally measured stiffness response from different structures within the specimen to match the stiffness regions identified in Figure 2. Average DIC displacements defined on equivalent RoIs (Figure 2a) were used to estimate the equivalent stiffnesses to K_1 and K_2, and allow comparisons with predicted values obtained from the two FE models (Figure 2b). Numerical FE predictions for K_{cement} were compared to the experimental stiffness values obtained from the cement cylinders. When considering the full vertebral construct, i.e. comprising the two cement end caps, the steel plate and VB, DIC led to an underestimate of the stiffness (denoted K_1 in Figure 2 and Table 2) compared from the value obtained from the load-displacement out of the materials testing machine, 1949 to 2947 Nmm^{-1} , respectively (Table 2). This difference mainly arises from the slight anterior rotation of the top cement end cap upon application of the load noticeable in the DIC images. As a result of this rotation the displacement of the anterior part of the end cap is greater than the displacement at the point of application of the load; this has the effect of leading to DIC to underestimate sample stiffness by about 34% of the actual value. On the other hand, the FE model with cement properties derived from experimental data matched the experimental stiffness for K_1 to within 3%, i.e. 2,844 Nmm^{-1} compared to 2,947 Nmm^{-1} ; while the same FE model, but this time with cement properties obtained from the literature, led to an overestimate of the construct stiffness by around 151%, i.e. 4,448 Nmm^{-1} compared to 2,947 Nmm^{-1} .

The use of DIC in the experimental part of this study allowed us to infer the contribution of the cement end caps to the total stiffness of the vertebral sample while affording additional validation steps to the FE models. DIC allowed an experimental estimate of the stiffness of the VB and bottom cement end cap (denoted K_2 in Figure 2 and Table 2). The FE model with cement properties derived from experimental data matched this to within 1%, i.e. 6,415 Nmm^{-1} compared to 6,484 Nmm^{-1} ; cement properties obtained from the literature were assigned in the FE model this led to a stiffness overestimate of around 124%, i.e. 8,060 Nmm^{-1} compared to 6,484 Nmm^{-1} .

The average stiffness of the 15 cement samples was found to be in the order of 141,160$\pm$33 Nmm^{-1} ; this value is approximately 26% higher than the predicted stiffness of the equivalent geometry volume of interest defined in the bottom cement end cap, denoted K_{cement} in Table 2, in the case of the model with cement properties obtained experimentally, while the model with cement properties inferred from the literature led to an overestimate of 190%, 105,110 Nmm^{-1} and 269,310 Nmm^{-1} , respectively. It is important to notice that K_{cement} in our models was calculated from the vertical displacement of a volume of interest defined within the cement end cap and loaded via the VB. As the cross-sectional geometry of the VB is not perfectly round it is inevitable that the volume of interest will contain elements which are not loaded, some of which are characterised by nodes exhibiting zero displacement, ultimately leading to an underestimate of the stiffness of the cement part. This is true independently of the properties assigned to this material in the model. This method of estimating cement stiffness is not expected to output results in good agreement with experimental data, however it gives an indication of whether the model behaviour is correct as it is expected to always lead to an underestimate of the stiffness value; the magnitude of this discrepancy being dependent on the level of cement coverage achieved while embedding the VB.

DIC allowed to isolate the contribution to overall specimen stiffness arising from different structures within the specimen and, by comparing experimental values to numerical predictions obtained from both models, it was found that the cement end caps accounted for most. However, when cement properties were assigned based on experimental data obtained from samples of equivalent geometry as the end caps and produced with a similar protocol, excellent agreement was obtained between experimental and numerical results.

Conclusion

In this study we have shown that precise setting of the material properties of bone cement will improve the accuracy of the FE stiffness predictions of vertebral samples. Therefore, it is recommended that an in-house characterisation of samples equivalent to the bone cement end cap fixtures is conducted to inform the correct properties to be assigned to this material in the model. Furthermore, we have outlined a technique which allows for robust model validation by exploiting the versatility of DIC measurements.

Conflict of interest

The authors do not have any conflict of interest.

Acknowledgement

We gratefully acknowledge the support of the Brazilian Government and CAPES for a PhD scholarship (Grant number 99999.001603/2015-09) and FAPESP (Grant number 2014/26366-4) for the initial support.

References

1. Blaber J, Adair B and Antoniou A (2015) Ncorr: Open-Source 2D Digital Image Correlation Matlab Software. *Experimental Mechanics* 55(6): 1105–1122.
2. British Standards Institution (2002) BS 5833:2002 Implants for surgery — Acrylic resin cements .
3. Buckley JM, Loo K and Motherway J (2007) Comparison of quantitative computed tomography-based measures in predicting vertebral compressive strength. *Bone* 40(3): 767–774.
4. Chandler M, Kowalski RSZ, Watkins ND, Briscoe A and New aMR (2006) Cementing techniques in hip resurfacing. *Proceedings of the Institution of Mechanical Engineers. Part H, Journal of engineering in medicine* 220(2): 321–331.
5. Chen Y, Dall'Ara E, Sales E, Manda K, Wallace R and Viceconti M (2017) Micro-CT based Finite Element Models of Cancellous bone predict accurately displacement once the boundary condition is well relicated: A validation study. *Journal of the Mechanical Behavior of Biomedical Materials* 65(September 2016): 644–651.
6. Chevalier Y, Charlebois M, Pahra D, Varga P, Heini P, Schneider E and Zysset P (2008) A patient-specific finite

element methodology to predict damage accumulation in vertebral bodies under axial compression, sagittal flexion and combined loads. *Computer methods in biomechanics and biomedical engineering* 11(5): 477–487.

7. Costa MC, Tozzi G, Cristofolini L, Danesi V, Viceconti M and Dall'Ara E (2017) Micro Finite Element models of the vertebral body: Validation of local displacement predictions. *PLoS One* 12(7): 1–18.
8. Crawford RP, Rosenberg WS and Keaveny TM (2003) Quantitative Computed Tomography-Based Finite Element Models of the Human Lumbar Vertebral Body: Effect of Element Size on Stiffness, Damage, and Fracture Strength Predictions. *Journal of Biomechanical Engineering* 125(4): 434.
9. Dall'Ara E, Varga P, Pahr D and Zysset P (2011) A calibration methodology of QCT BMD for human vertebral body with registered micro-CT images. *Medical Physics* 38(5): 2602–2608.
10. Eswaran SK, Gupta A and Keaveny TM (2007) Locations of bone tissue at high risk of initial failure during compressive loading of the human vertebral body. *Bone* 41(4): 733–739.
11. Eyerer P and Jin R (1986) Influence of mixing technique on some properties of PMMA bone cement. *Journal of Biomedical Materials Research* 20(8): 1057–1094.
12. Gustafson H, Siegmund G and Cripton P (2016) Comparison of Strain Rosettes and Digital Image Correlation for Measuring Vertebral Body Strain. *Journal of Biomechanical Engineering* 138(5).
13. Gustafson HM and Cripton PA (2013) Use of Digital Image Correlation for Validation of Surface Strain in Specimen-specific Vertebral Finite Element Models. *Proceedings of the 9th Ohio State University Injury Biomechanics Symposium* : 1–11.
14. Gustafson HM, Cripton PA, Ferguson SJ and Helgason B (2017) Comparison of specimen-specific vertebral body finite element models with experimental digital image correlation measurements. *Journal of the Mechanical Behavior of Biomedical Materials* 65(October 2016): 801–807.
15. Hernandez BA (2019) *A study of impact loading of the spine*. PhD Thesis, University of Bath.
16. Hernandez BA, Gill HS and Gheduzzi S (2018) Taguchi analysis of factors affecting finite element modelling of vertebral bodies. In: *8th World Congress of Biomechanics*. 8th World Congress of Biomechanics.
17. Hosseini HS, Clouthier AL and Zysset PK (2014) Experimental validation of finite element analysis of human vertebral collapse under large compressive strains. *Journal of biomechanical engineering* 136(4): 041006.
18. Jones AC and Wilcox RK (2007) Assessment of Factors Influencing Finite Element Vertebral Model Predictions. *Convergence* 129(December): 2–7.
19. Jones AC and Wilcox RK (2008) Finite element analysis of the spine: Towards a framework of verification, validation and sensitivity analysis. *Medical Engineering and Physics* 30(10): 1287–1304.
20. Kopperdahl D, Morgan E and Keaveny T (2002) Quantitative computed tomography estimates of the mechanical properties of human vertebral trabecular bone. *J Orthop Res* 20: 801–805.
21. Kopperdahl DL, Aspelund T, Hoffmann PF, Sigurdsson S, Siggeirsdottir K, Harris TB, Gudnason V and Keaveny TM (2014) Assessment of incident spine and hip fractures in women and men using finite element analysis of CT scans. *Journal of Bone and Mineral Research* 29(3): 570–580.
22. Lee C (2005) Properties of Bone Cement : The Mechanical Properties of PMMA Bone Cement. *The Well-Cemented Total Hip Arthroplasty* : 60–66.
23. Lewis G (1997) Properties of acrylic bone cement: state of the art review. *Journal of biomedical materials research* 38(May 1996): 155–82.
24. Macaulay W, DiGiovanni CW, Restrepo A, Saleh KJ, Walsh H, Crossett LS, Peterson MG, Li S and Salvati EA (2002) Differences in bone-cement porosity by vacuum mixing, centrifugation, and hand mixing. *Journal of Arthroplasty* 17(5): 569–575.
25. Maquer G, Dall'Ara E and Zysset PK (2012) Removal of the cortical endplates has little effect on ultimate load and damage distribution in QCT-based voxel models of human lumbar vertebrae under axial compression. *Journal of Biomechanics* 45(9): 1733–1738.
26. Maquer G, Laurent M, Brandejsky V, Pretterklieber ML and Zysset PK (2014) Finite Element Based Nonlinear Normalization of Human Lumbar Intervertebral Disc Stiffness to Account for Its Morphology. *Journal of Biomechanical Engineering* 136(6): 061003.
27. Mengoni M, Vasiljeva K, Jones AC, Tarsuslugil SM and Wilcox RK (2016) Subject-specific multi-validation of a finite element model of ovine cervical functional spinal units. *Journal of Biomechanics* 49(2): 259–266.
28. Messick KJ, Miller MA, Damron LA, Race A, Clarke MT and Mann KA (2007) Vacuum-mixing cement does not decrease overall porosity in cemented femoral stems: An in vitro laboratory investigation. *Journal of Bone and Joint Surgery - Series B* 89(8): 1115–1121.
29. Mullins LP, Bruzzi MS and McHugh PE (2009) Calibration of a constitutive model for the post-yield behaviour of cortical bone. *Journal of the Mechanical Behavior of Biomedical Materials* 2(5): 460–470.
30. Newell N, Little JP, Christou A, Adams MA, Adam CJ and Masouros SD (2017) Biomechanics of the human intervertebral disc: A review of testing techniques and results. *Journal of the Mechanical Behavior of Biomedical Materials* 69(August 2016): 420–434.
31. Pahr DH, Schwiedrzik J, Dall'Ara E and Zysset PK (2014) Clinical versus pre-clinical FE models for vertebral body strength predictions. *Journal of the Mechanical Behavior of Biomedical Materials* 33(1): 76–83.
32. Palanca M, Brugo TM and Cristofolini L (2015) Use of digital image correlation to investigate the biomechanics of the vertebra. *Journal of Mechanics in Medicine and Biology* 15(2): 1–10.
33. Palanca M, Tozzi G and Cristofolini L (2016) The use of digital image correlation in the biomechanical area: A review. *International Biomechanics* 3(1): 1–21.
34. Race A, Mann KA and Edidin AA (2007) Mechanics of bone/PMMA composite structures: An in vitro study of human vertebrae. *Journal of Biomechanics* 40(5): 1002–1010.
35. Reutlinger C, Bürki A, Brandejsky V, Ebert L and Büchler P (2014) Specimen specific parameter identification of ovine lumbar intervertebral discs: On the influence of fibre-matrix and fibre-fibre shear interactions. *Journal of the Mechanical Behavior of Biomedical Materials* 30: 279–289.

36. Robson Brown K, Tarsuslugil S, Wijayathunga VN and Wilcox RK (2014) Comparative finite-element analysis: a single computational modelling method can estimate the mechanical properties of porcine and human vertebrae. *Journal of the Royal Society, Interface / the Royal Society* 11(95).
37. Rohlmann A, Burra NK, Zander T and Bergmann G (2007) Comparison of the effects of bilateral posterior dynamic and rigid fixation devices on the loads in the lumbar spine: A finite element analysis. *European Spine Journal* 16(8): 1223–1231.
38. Ruspi ML, Palanca M, Faldini C and Cristofolini L (2017) Full-field in vitro investigation of hard and soft tissue strain in the spine by means of Digital Image Correlation. *Muscles, ligaments and tendons journal* 7(4): 538–545.
39. Saha S and Pal S (1984) Mechanical properties of bone cement: A review. *Journal of Biomedical Materials Research* 18(4): 435–462.
40. Sahli F, Cuellar J, Pérez A, Fields AJ, Campos M and Ramos-Grez J (2015) Structural parameters determining the strength of the porcine vertebral body affected by tumours. *Computer Methods in Biomechanics and Biomedical Engineering* 18(8): 890–899.
41. Synopsys (2016) Variability and Accuracy of Spine Segmentation.
42. Taylor J (1997) *Introduction to Error Analysis, the Study of Uncertainties in Physical Measurements*. 2nd edition. New York: University Science Books.
43. Teo EC and Ng HW (2001) Evaluation of the role of ligaments, facets and disc nucleus in lower cervical spine under compression and sagittal moments using finite element method. *Medical Engineering and Physics* 23(3): 155–164.
44. Tozzi G, Danesi V, Palanca M and Cristofolini L (2016) Elastic Full-Field Strain Analysis and Microdamage Progression in the Vertebral Body from Digital Volume Correlation. *Strain* 52(5): 446–455.
45. Wijayathunga VN, Jones AC, Oakland RJ, Furtado NR, Hall RM and Wilcox RK (2008) Development of specimen-specific finite element models of human vertebrae for the analysis of vertebroplasty. *Proceedings of the Institution of Mechanical Engineers, Part H: Journal of Engineering in Medicine* 222(2): 221–228.